Published by Institute of Physics Publishing for SISSA

Received: *Febraury 01, 2007*
Accepted: *August 15, 2007*
Published: *August 27, 2007*

Neutrino beams from electron capture at high gamma

Mark Rolinec

Physik-Department, Technische Universität München,
James-Franck-Strasse, 85748 Garching, Germany
E-mail: rolinec@ph.tum.de

Joe Sato

Department of Physics, Saitama University,
Shimo-okubo, Sakura-ku, Saitama, 338-8570, Japan
E-mail: joe@phy.saitama-u.ac.jp

Abstract: We investigate the potential of a flavor pure high gamma electron capture electron neutrino beam directed towards a large Water Cherenkov detector with 500 kt fiducial mass. The energy of the neutrinos is reconstructed by the position measurement within the detector and superb energy resolution capabilities could be achieved. We estimate the requirements for such a scenario to be competitive to a neutrino/anti-neutrino running at a neutrino factory with less accurate energy resolution. Although the requirements turn out to be extreme, in principle such a scenario could achieve as good abilities to resolve correlations and degeneracies in the search for $\sin^2 2\theta_{13}$ and $\delta_{\rm CP}$ as a standard neutrino factory experiment.

Keywords: CP violation, Neutrino Physics, Beyond Standard Model.

JHEP08(2007)079

Contents

JHEP08(2007)079

1. Introduction

All observations on neutrinos coming from the sun [1 – 10], the atmosphere [11 – 18], and reactors [19, 20] are well understood in the picture of neutrino oscillations [21] in the three generation framework of lepton mixing. Two of the mixing angles, $\sin^2 2\theta_{12}$ and $\sin^2 2\theta_{23}$ have been measured as well as the two mass square differences $|\Delta m^2_{31}|$ and Δm^2_{21} have been determined. Furthermore, the parameters which are mainly relevant in the atmospheric neutrino oscillations, i.e. $\sin^2 2\theta_{23}$ and $|\Delta m^2_{31}|$ have been confirmed by the terrestrial experiments K2K [22 – 24] and MINOS [25, 26].

However, the remaining two mixing parameters, the third mixing angle $\sin^2 2\theta_{13}$ and the CP violating phase $\delta_{\rm CP}$ have not been determined yet. Currently, there only exists an upper bound for $\sin^2 2\theta_{13}$ [27, 28] and there is no information on the value of $\delta_{\rm CP}$. Also, the sign of the mass squared difference Δm^2_{31} is currently unknown, i.e. it is unclear if neutrinos exist in normal or inverted hierarchy. So, the aim of future oscillation experiments is to measure these two parameters, to improve the precision to the leading solar and atmospheric parameters, and determine the neutrino mass hierarchy. In order to complete the picture of neutrino oscillation parameters, several types of new experiments have been proposed and are studied extensively. This includes reactor experiments [29 – 34] that are only sensitive to $\sin^2 2\theta_{13}$, and experiments where information on both, $\sin^2 2\theta_{13}$ and $\delta_{\rm CP}$ can be obtained, like superbeam experiments [35 – 40], neutrino factories [41 – 49], and beta-beams [50 – 63].

Recently, another idea has been proposed, which makes use of a neutrino beam with neutrinos coming from electron capture processes [64, 65]. The electron neutrinos that are emitted from such electron capture processes would have a definite energy Q in the rest frame of the mother nuclei. Therefore by accelerating the mother nuclei to a Lorentz factor γ the neutrino energy E_ν can be completely controlled, since the energy of the neutrinos that are boosted exactly towards the direction of the detector is $\mathrm{E}_\nu = 2\gamma Q$. So, the γ factor and the baseline length L have to be chosen respectively to the Q value of the electron capture process, the location of the oscillation maximum, and the minimal energy observable at the detector, e.g. above the Cherenkov threshold of muons at a Water Cherenkov detector. For example, if Q is relatively large ($\mathcal{O}(1\,\mathrm{MeV})$), γ can be chosen to be of the order $\mathcal{O}(100)$. In this case the neutrino beam can be viewed as exactly monoenergetic in the detector [63 – 70]. On the contrary, if Q is relatively small ($\mathcal{O}(100\ \mathrm{keV})$) the γ must be chosen quite high ($\mathcal{O}(1000)$), but the necessary choice of the baseline leads to the effect that the neutrinos now have a wider energy range at the detector. While the maximal energy of $\mathrm{E}_\nu = 2\gamma Q$ is reached by the neutrinos in the beam axis, the energy of the neutrinos becomes smaller off the axis and the minimal observable energy of the neutrinos depends on the detector size and the baseline. In this scenario, the neutrino energy can be reconstructed from the vertex position measurement relatively to the beam axis within the detector and in principle a superb energy resolution can be achieved [64, 66]. This however requires in addition to the resolution of the position measurement within the detector, that the beam divergence of the stored mother nuclei can be accurately controlled. This scenario seems interesting since only with one acceleration factor γ a wide range of neutrino energy can be covered simultaneously with a very accurate neutrino energy determination.

In this work we investigate the potential of such scenarios with a flavor pure electron neutrino beam coming from beta capture at high γ lead towards a Water Cherenkov detector with a fiducial mass of 500 kt. We will refer to these scenarios as monobeam scenarios in the following. We estimate the requirements for such a scenario to be able to resolve correlations and degeneracies in the search for the remaining oscillation parameters $\sin^2 2\theta_{13}$ and δ_{CP} within the measurement in only one polarity, i.e. neutrino running, but with superb energy resolution abilities and to be competitive to a standard neutrino factory scenario with neutrino and anti-neutrino running, but less accurate energy reconstruction. Unfortunately, the ability to also gain information on the sign of Δm^2_{31} at the discussed monobeam scenarios is limited due to the missing anti-neutrino running, so it will be omitted throughout this work.

This work is organized as follows: in section 2 we sketch the basic principles of the high gamma electron capture monobeam experiments and summarize all underlying assumptions. Furthermore, we define the reference setups that are investigated throughout the rest of the work. Next, in section 3 we address the issue of requirements to resolve parameter correlations and degeneracies in the sensitivity to $\sin^2 2\theta_{13}$ at the reference scenarios defined in section 2 and then address the sensitivity to δ_{CP} in section 4. Here, also all parameter correlations and degeneracies are taken into account. We summarize and conclude the main results in section 5. Finally, the details of the operation of a monobeam experiment including the energy reconstruction by the position measurement, i.e. a deriva-

JHEP08(2007)079

tion of the neutrino energy $E_\nu(R)$ as a function of the radius from the beam axis, and the details of the event rate calculation is presented in the appendix.

2. Experiment configurations and simulation techniques

In the scope of this work we consider a flavor pure neutrino beam that is produced within the electron capture process of $^{110}_{50}$Sn isotopes:

$$^{110}_{50}\mathrm{Sn} + \mathrm{e}^- \rightarrow {}^{110}_{49}\mathrm{In} + \nu_\mathrm{e}. \tag{2.1}$$

In the rest frame of the process the produced neutrinos are monochromatic with an energy of Q = 267 keV[1] at a lifetime of 4.11 h[2]. The isotopes are assumed to be accelerated in a decay ring, where they coincide with electrons accelerated at the same γ factor and a boosted neutrino beam is produced towards the detector. At the distance of the baseline L the neutrinos hit the detector at a radial distance R from the beam axis and their energy in the laboratory frame (rest frame of the detector) can be expressed as

$$E_\nu(R) = \frac{Q}{\gamma}\left[1 - \frac{\beta}{\sqrt{1+(R/L)^2}}\right]^{-1} \approx \frac{2\gamma Q}{1+(\gamma R/L)^2}. \tag{2.2}$$

The derivation of this formula can be found in the appendix, whereas the approximation is taken from [64] and can be obtained in the limit of large γ with $\beta \approx 1 - \frac{1}{2\gamma^2}$ and $(R/L) \ll 1$. At the beam center the neutrino energy is maximal at a value of $E_\nu = 2\gamma Q$ and decreases for larger distances from the beam center. Since the neutrino energy is a function of the distance from the beam center, a position measurement within the detector allows a precise reconstruction of the neutrino energy. We assume a Water Cherenkov detector with a fiducial mass of 500 kt. The large detector mass allows to collect enough statistics that is needed to gain from the superb energy resolution and can have large geometrical size in order to have a enough broad energy window, since the minimal measurable energy depends on the maximal distance from the beam center. We assume the geometry of the detector to be as shown in figure 1. The radius of the detector is set to $R_\mathrm{max} = 100\,\mathrm{m}$ so that the depth is still approximately 64 m and a reconstruction of the Cherenkov rings and electron/muon identification remains possible. The position measurement should be optimized for this kind of experimental setup and reach at least a resolution of ΔR =30 cm, which has been the estimated vertex resolution at Super-K for fully-contained single ring

[1]We only consider electron capture from the K shell here. A more detailed analysis should also include electron capture from higher shells. However, the results should not be affected significantly. On one hand a position measurement of a neutrino would allow different true energy values and a new discrete uncertainty arises, but on the other hand the ratio is known and the higher the shell, the smaller the contribution. Furthermore, the sets of neutrinos from electron captures from other shells cannot be interpreted as background since also their energy is accurately known, besides a discrete uncertainty, and they also oscillate and hence contribute to the fit.

[2]This is the main limiting factor for obtaining an adequate number of electron capture processes per year, i.e. to collect enough statistics. However, in [71 – 73] the possibility to enhance the electron capture rate has been discussed.

JHEP08(2007)079

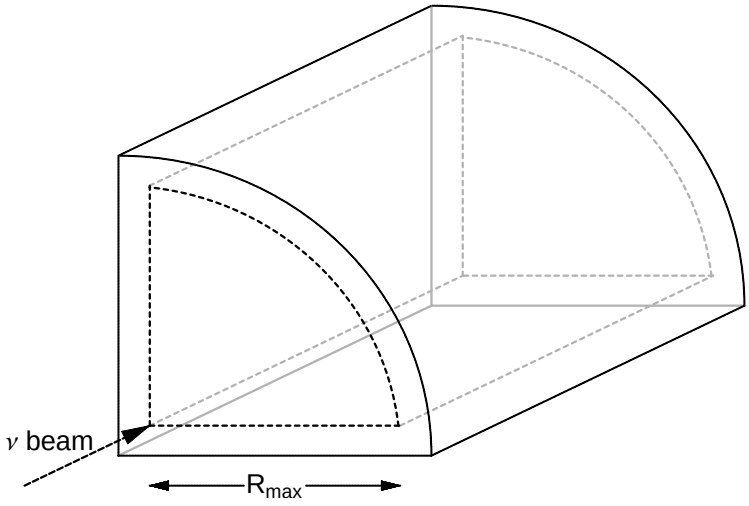

Figure 1: Scheme of the detector setting. The fiducial volume is indicated by the dashed lines. The neutrino beam hits the detector at the edge of the fiducial volume to allow for distance measurements from the beam axis. In case of $R_{\max} = 100\,\mathrm{m}$ the depth of the fiducial volume part would be approximately 64 m for a 500 kt fiducial detector mass.

events [14]. Furthermore, the vertex resolution for muon events, i.e. the monobeam signal events, is slightly better than for electron events and can even reach a resolution of 25 cm in the energy window of interest. It should be mentioned that the very good position measurement resolution can only be transfered into an excellent energy resolution if the systematical uncertainty in the beam spread can be reasonably controlled. This means that the divergence of the stored isotopes perpendicular to the beam line must satisfy the condition $p_x/p_z \lesssim \Delta R/L$ before the decay. Otherwise, the superb energy resolution that is assumed in this work could not be achieved although the position measurement is accurate. This translates for baselines that are discussed in the following into the requirement of a beam divergence $p_x/p_z \lesssim 1$ μrad for the mother nuclei in the storage ring and seems hardly feasible. However, it should be noted that beam divergences of $\mathcal{O}(1$ μrad) are already discussed, for instance for the proton beam of the LHC for the operation of the TOTEM experiment [74].

For having neutrino energies beyond the Cherenkov threshold and allow for electron/muon discrimination, we only discuss monobeam setups with neutrino energies above 400 MeV. The signal efficiencies and background rejection factors follow the analysis from [54] (mainly the low gamma beta beam therein). Above 400 MeV up to 700 MeV there was found a signal efficiency of approximately 0.55 for the appearance measurement of muon neutrinos, which we take to be the signal efficiency of the discussed monobeam scenarios. Although the signal efficiency in [54] decreases slightly for higher neutrino energies, we assume the signal efficiency to stay stable up to the highest energies discussed in this work ($\mathrm{E}_\nu \lesssim 1.4\,\mathrm{GeV}$), since the monobeam setup does not rely on the quasi-elastic events only, because the energy reconstruction can be performed by the position measurement

JHEP08(2007)079

within the detector. The rejection factors for background coming from neutral current events with single pion production at energies above 400 MeV are found to be below 10^{-3} in [54], whereas we assume this background rejection to be at a level of 10^{-4}. This is a quite optimistic assumption, and it is not clear, that this could be achieved. However, note that the mismatch of ordinary energy reconstruction and energy reconstruction by position measurement due to the carried away missing energy of the neutrino in neutral current reactions could give a further rejection ability of such background events. We assume a systematical uncertainty of 2.5% for the signal events and 5% for the background events, as also assumed for the typical beta beam scenarios, i.e. in [61]. The uncertainty of the signal events has probably to be called optimistic, but since we will find that the main effect will come from correlations and degeneracies [75 – 77], a value of 5% would not have much impact to the results of this work.

As can be understood from eq. (2.2), the energy window of the analysis is, due to the technique of energy reconstruction, limited by the size of the detector to the interval

$$\frac{2\gamma Q}{1+(\gamma R_{\max}/L)^2} \leq E_\nu \leq 2\gamma Q, \tag{2.3}$$

so that the energy window is completely fixed after the baseline L and the acceleration factor of the ions γ is chosen. So finding an optimal Setup is more complicated as it is for example in the case of beta beams, since choosing a perfect pair of L and γ to exactly measure at the first oscillation maximum can suffer from an energy window that is to small to allow resolving correlations and degeneracies. However, adjusting the baseline to smaller baselines in order to have a lower minimal energy also shifts the oscillation maximum to lower energies, while going to higher values of γ not only shifts the maximal energy but also the minimal energy to higher values. So, the whole energy window moves away from the oscillation maximum although it is broadened. Therefore, in the next sections we discuss the potential and performance of the following different reference scenarios of monobeam setups:

- **Setup I**: The Water Cherenkov detector with a fiducial mass of 500 kt is located at a baseline of L=600km, the mother nuclei $^{110}_{50}$Sn are accelerated with $\gamma = 2500$ and 10 years of data taking are assumed at the number of 10^{18} electron capture decays per year.

- **Setup II**: The Water Cherenkov detector with a fiducial mass of 500 kt is located at a baseline of L=250km, the mother nuclei $^{110}_{50}$Sn are accelerated with $\gamma = 2000$ and 10 years of data taking are assumed at the number of 10^{18} electron capture decays per year

- **Setup III**: The Water Cherenkov detector with a fiducial mass of 500 kt is located at a baseline of L=600km, the mother nuclei $^{110}_{50}$Sn are accelerated with $\gamma = 900$ and $\gamma = 2500$ consecutively, and 5 years of data taking are assumed in each of the two phases so that as for Setup I and II the total running time is 10 years. The number of 10^{18} electron capture decays per year is assumed for both phases.

JHEP08(2007)079

Setup I is located at the first oscillation maximum, but the energy window is not very broad compared to the width oft the oscillation maximum peak, therefore we also discuss the second scenario, Setup II, with a broader energy window which on the other hand is located slightly off the first oscillation maximum at higher neutrino energies due to the smaller baseline. Then again, because of the smaller baseline higher event rates can be obtained at Setup II. With Setup III we discuss the potential in resolving the correlations and degeneracies with a monobeam experiment by a combination of data from the first oscillation maximum and also the second oscillation maximum. This combination should be a powerful tool to resolve the degeneracies and the importance of the second oscillation maximum has been discussed in [78]. Since the first oscillation maximum phase at Setup III is comparable to Setup I, the gain from the additional measurement at the second oscillation maximum can directly be read off the comparison of Setup I and Setup III. The exact width of the corresponding energy windows of the setups and their location respectively to the oscillation maxima are shown in figure 2. Note, that Setup III makes use of the combination of different γ which was also the strategy for the "high Q-low γ" electron capture beam experiment scenarios as discussed in [65, 67 – 70]. However, for these scenarios this strategy was required to obtain spectral information at the first oscillation maximum, while Setup III provides spectral information at the higher $\gamma = 2500$ and information from the second oscillation maximum is included with the second arrangement of $\gamma = 900$. This can be seen in figure 2.

There, the appearance probability $\mathrm{P}(\nu_\mathrm{e} \to \nu_\mu)$ is plotted for $\sin^2 2\theta_{13} = 0.01$ and three choices of δ_CP (the other oscillation parameters are chosen as in eq. (2.4)). The yellow (grey) bands indicate the energy window of the analysis for Setup I and III in the left-hand side and Setup II in the right-hand side. It can be seen that the energy window for the choice of L=600km and $\gamma = 900$ is essentially only a very narrow band while for the higher values of γ indeed a broader energy window can be covered over the whole radius of the detector. However, the energy window of Setup I is too narrow to cover the first oscillation maximum for the different choices of δ_CP. For $\delta_\mathrm{CP} = 0$ the peak of the first oscillation maximum lies inside the energy window of the analysis but for the maximally CP violating values for δ_CP the peak moves outside the energy window. The energy window of Setup II lies above the first oscillation maximum independent of δ_CP but we will show in the next sections that Setup I will suffer more from correlations and degeneracies than Setup II since the latter benefits from a higher event rate due to the smaller baseline and the larger energy window, where the superb energy resolution can evolve.

Note, that the number of electron capture decays per year taken for the reference scenarios is of the order of the "high Q" electron capture scenarios discussed in [65, 67 – 70] and also the order of beta decays per year discussed for the beta beam scenarios [50 – 62]. However, because of the long lifetime of the $^{110}_{50}$Sn electron capture of 4.11 h in the rest frame the feasibility to achieve a number of 10^{18} per year seems out of range if it cannot be enhanced. This enhancement of the electron capture processes could be achieved by a laser irradiation as discussed in [71 – 73]. Furthermore, as is also the case for high gamma beta beams [54, 61] the high gamma values require a very large accelerator complex of the size of the LHC.

JHEP08(2007)079

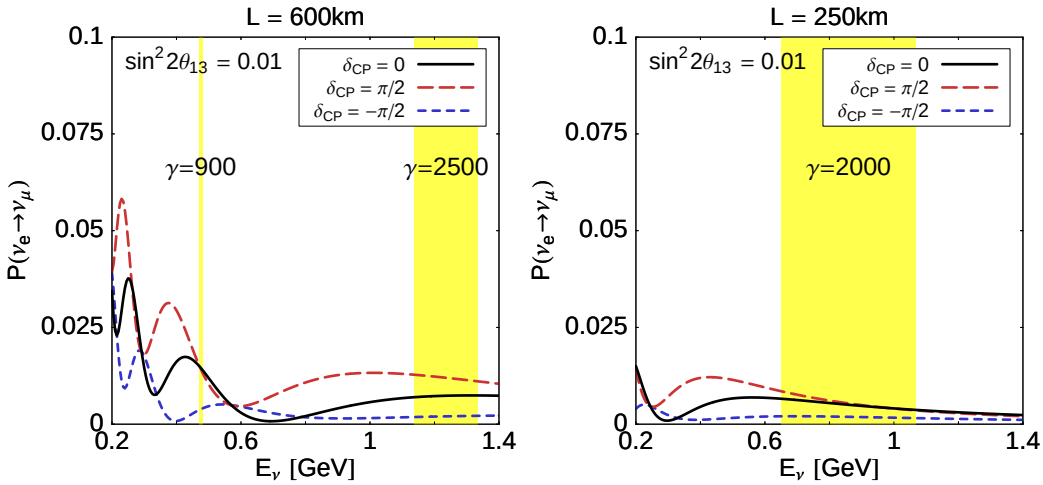

Figure 2: The appearance probability $P(\nu_e \to \nu_\mu)$ as a function of the neutrino energy E_ν at a baseline of L=250km (left-hand side) and L=600km (right-hand side). The oscillation parameter values are the ones from eq. (2.4), $\sin^2 2\theta = 0.01$ and the values for the phase δ_{CP} are chosen as labeled in the plot legend. The vertical yellow (grey) bands indicate the energy window of the analysis that is given for a detector radius of $R_{\max} = 100$m, the respective baseline L and the chosen γ factors, i.e. $\gamma = 900/\gamma = 2500$ for the scenarios at L=600km (Setup I and Setup III) and $\gamma = 2000$ for the scenario at L=250km (Setup II).

For reasons of comparison and to put the performance of the monobeam setups into perspective we will compare the results to a standard neutrino factory setup with a 50 kt MID detector at a baseline of L=3000km and a parent energy of the stored muons $E_\mu =$ 50GeV. This neutrino factory setup is similar to the standard scenario for a neutrino experiment [45], commonly known as NuFact-II, with $1.06 \cdot 10^{21}$ useful muon decays per year (corresponding to $5.3{\cdot}10^{20}$ useful muon decays per year and polarity for a simultaneous operation with both polarities). The details of the neutrino factory experiment description follow the description of the NuFact-II scenario in [49]. We assume a runtime of five years in each polarity, so that the total running time is 10 years as for the discussed monobeam setups. Furthermore we will also consider an optimized neutrino factory scenario at the end of section 4, where compared to the standard neutrino factory scenario a second detector similar to the standard detector at L=3000km is installed at the magic baseline L=7500km.[3]

The analysis throughout this work is performed with the GLoBES software [80, 81] and the incorporated Poisson χ^2-analysis. Details can be found in the GLoBES manual [82]. Since the monobeam only measures ν_μ-appearance and could additionally only observe ν_e-disappearance, the leading atmospheric parameters $\sin^2 2\theta_{23}$ and $|\Delta m^2_{31}|$ cannot be determined as would be the case at a neutrino factory with a measurement in the ν_μ-

[3]The optimized scenario furthermore uses an optimized disappearance channel with the MINOS energy threshold [38] while the muon CID with the implied CID cut threshold is only used for the golden appearance channel. See [79] for details.

JHEP08(2007)079

disappearance channel. Thus, correlations with the leading atmospheric parameters would spoil the potential of the monobeam experiment alone, as also would be the case for a beta beam for the same reasons. Therfore, we adopt the same technique as in [61] and add the ν_μ-disappearance information from a simulation of the superbeam experiment T2K. The corresponding appearance information is excluded, so that information on $\sin^2 2\theta_{13}$ and $\delta_{\rm CP}$ is solely collected by the monobeam experiment (see [61] for details). The errors on the solar parameters are taken to be 5% on each, Δm^2_{21} and θ_{12}.

As input or so-called true values within the simulations, we use, unless stated otherwise the following parameter values, close to the current best fit values (see refs. [83 – 86]):

$$\begin{aligned} \Delta m^2_{31} &= 2.5 \cdot 10^{-3}\,\mathrm{eV}^2 \quad \sin^2 2\theta_{23} = 1.0\,, \\ \Delta m^2_{21} &= 8.2 \cdot 10^{-5}\,\mathrm{eV}^2 \quad \sin^2 2\theta_{12} = 0.83. \end{aligned} \tag{2.4}$$

Note, that the octant-degeneracy [87] does not affect our results, since we choose $\sin^2 2\theta_{23}$ to be maximal and thus the octant-degenerate solution appears at the same point in the parameter space as the original solution in the parameter space. So, if it is stated that effects of degeneracies are taken into account in the analysis, only the intrinsic $\sin^2 2\theta_{13}$-$\delta_{\rm CP}$-degeneracy [88] and the sign(Δm^2_{31})-degeneracy [76] are regarded out of the complete set of the so-called eight-fold degeneracy [77].

3. Sensitivity to $\sin^2 2\theta_{13}$

The sensitivity to $\sin^2 2\theta_{13}$ is calculated under the hypothesis of true $\sin^2 2\theta_{13} = 0$. The sensitivity limit at a certain confidence level is then the maximal fit value of $\sin^2 2\theta_{13}$ that still fits the simulated data at the chosen confidence level, i.e. it would be the lower bound to $\sin^2 2\theta_{13}$ that the experiment could achieve in case of vanishing true $\sin^2 2\theta_{13}$. It is well known, that the main problem is to resolve the correlations with the other oscillation parameters and the so-called eight-fold degeneracy. In figure 3 the sensitivity to $\sin^2 2\theta_{13}$ is shown at the 3σ confidence level as a function of the number of decays per year for the monobeam scenarios at L=600km/γ = 2500, L=250km/γ = 2000, and L=600km/γ = 900+γ = 2500. The vertical lines indicate the reference setups at a number of 10^{18} ion decays per year. In each plot the lowest curve represents the pure statistical limit to θ and the colored bands show how the sensitivity degrades if also systematics (blue/dark grey band), correlations (green/middle grey band), and degeneracies (yellow/bright grey band) are taken into account. The final achievable sensitivity limit to $\sin^2 2\theta_{13}$ is given by the upper curve. Obviously the statistical and systematical sensitivity limit to $\sin^2 2\theta_{13}$ at all three scenarios in figure 3 can reach to very small values of $\sin^2 2\theta_{13}$ due to the very large statistics in the Water Cherenkov detector. However, the monobeam scenario at L=600km/γ = 2500 can resolve the correlations not until an exposure of 10^{17} decays per year. The point where the degeneracies can be resolved is reached not until approximately 10^{20} decays per year, which of course is beyond any feasibility. So despite the improvement of the statistical limit with higher exposures the final sensitivity limit to $\sin^2 2\theta_{13}$ stays relatively stable a approximately $\sin^2 2\theta_{13} \approx 10^{-2}$ independent of the number of decays per

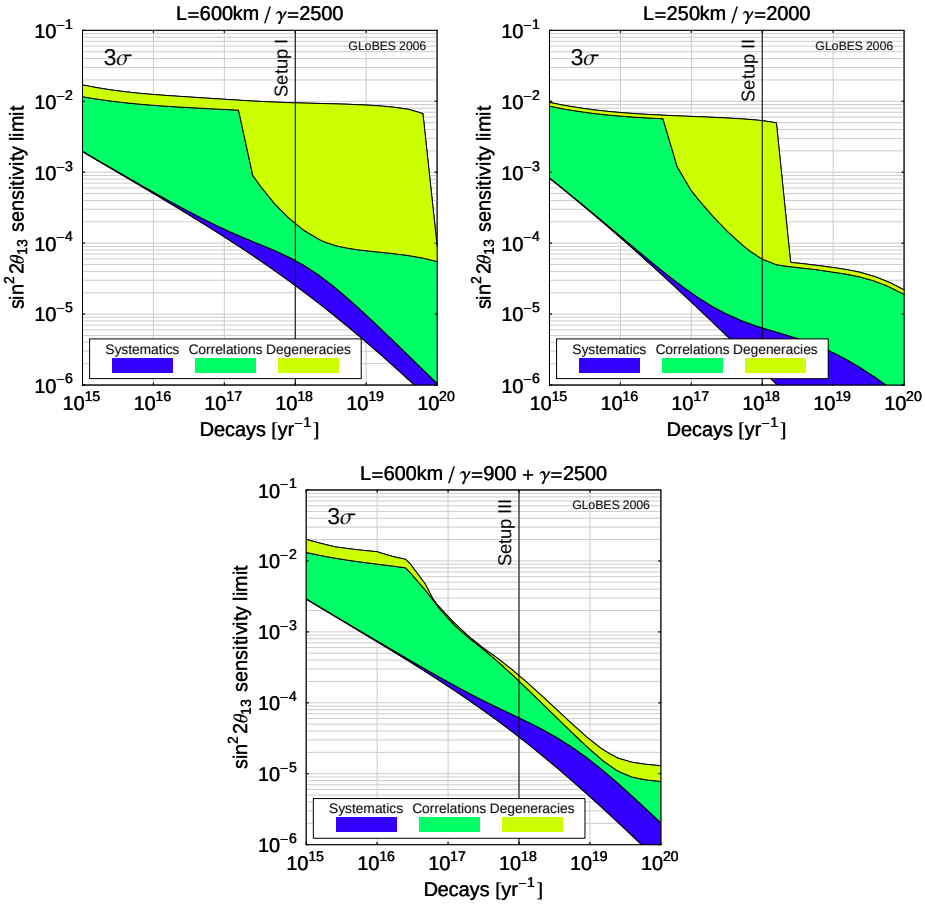

Figure 3: The sensitivity to $\sin^2 2\theta_{13}$ at the 3σ confidence level for the monobeam scenarios L=600km/$\gamma = 2500$, L=250km/$\gamma = 2000$, and L=600km/$\gamma = 900 + \gamma = 2500$ as a function of the number of decaying ions per year including statistics, systematics, correlations, and degeneracies. The lowest curve represents the pure statistical sensitivity limit to $\sin^2 2\theta_{13}$ and the colored bands indicate the effect of switching on systematics (blue/dark grey), correlations (green/middle grey), and degeneracies (yellow/bright grey) so that the final sensitivity limit is given by the upper curve.

year. The monobeam scenario at a baseline of L=250km and $\gamma = 2000$ suffers from the same problem. First, the sensitivity limit does only slightly improve and almost stays stable. Beyond exposures of 10^{18} decays per year this scenario starts to resolve the degeneracies and the sensitivity limit to $\sin^2 2\theta_{13}$ improves significantly. From figure 3 it becomes clear, that the technique of a high gamma monobeam with its superb energy resolution in a narrow energy window is not able to resolve the correlations and degeneracies in a measurement at just one γ. The scenario at a baseline of L=600km allows to measure in the second oscillation maximum since for L=600km this maximum is located above the Cherenkov threshold and events can be collected. The lower plot of figure 3 shows the sensitivity limit to $\sin^2 2\theta_{13}$ for such a scenario, where 5 years data taking at $\gamma = 900$ and 5 years data taking at $\gamma = 2500$ is combined. Now, the correlations and degeneracies can be already

JHEP08(2007)079

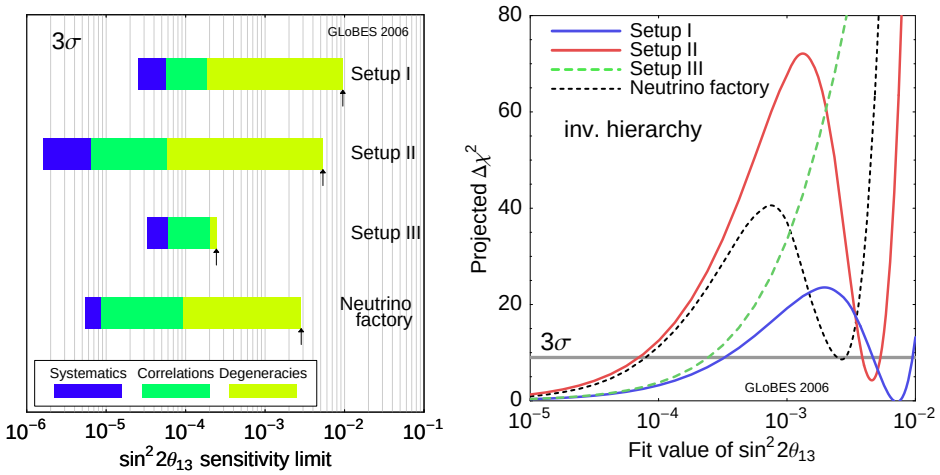

Figure 4: Left-hand side: comparison of the sensitivity to $\sin^2 2\theta_{13}$ at the 3σ confidence level at the monobeam scenarios Setup I, Setup II, Setup II, and a neutrino factory at a baseline of L=3000km including systematics, correlations and degeneracies. The left edge of the bars indicates a pure statistical sensitivity limit. The right edges of the bars indicate the sensitivity limit after switching on systematics (blue/dark grey), correlations (green/middle grey), and correlations (yellow/bright grey), so that the rightmost edge gives the final sensitivity limit to $\sin^2 2\theta_{13}$. Right-hand side: the projected $\Delta\chi^2$ as a function of the fit value of $\sin^2 2\theta_{13}$ fitted under the assumption of inverted hierarchy while the true values are given with $\sin^2 2\theta_{13}$ and normal hierarchy. The rightmost intersections of the curves with the grey horizontal 3σ line give the right edges of the bars in the plot on the left-hand side.

resolved for lower exposures. We checked that it is not necessary to split up the two data taking phases into an equal period of five years each. The ability to resolve the correlations and degeneracies still remains if only 2 years data taking at $\gamma = 900$ are combined with 8 years at $\gamma = 2500$ and the final sensitivity would be even slightly better since then more statistics could be collected at the first oscillation maximum.

For reasons of comparison, the sensitivity to $\sin^2 2\theta_{13}$ at Setup I, Setup II, and Setup III are again shown in the left-hand side of figure 4 and confronted with the sensitivity limit obtainable at the standard neutrino factory scenario. The neutrino factory also suffers from the correlations and degeneracies. But as can be seen in the right-hand side of figure 4 the difference is that the neutrino factory can almost resolve the degenerate solution. There, the projected $\Delta\chi^2$ is shown as a function of the fit value of $\sin^2 2\theta_{13}$ for the degenerate solution with the wrong sign, i.e. inverted hierarchy while the positive Δm^2_{31} was taken as input true value. The degenerate solution appears for the neutrino factory scenario at a $\Delta\chi^2$ only slightly below the 3σ, while the degenerate solution for Setup I appears at $\Delta\chi^2 = 0$ and thus fits as good as $\sin^2 2\theta_{13} = 0$. On the other hand, with Setup III there does not appear a second local minimum in the projected $\Delta\chi^2$ so the combination of first and second oscillation maximum data gives a strong tool to resolve the degeneracy. However, resolving the degeneracies remains the main problem if one want to reach to very small values of $\sin^2 2\theta_{13}$ and one could also think of a combination of a monobeam setups

JHEP08(2007)079

with the anti-neutrino running of a standard beta beam scenario. It should be noted that the performance of a neutrino factory could be improved by additional data from the silver channel $\nu_\mu \to \nu_\tau$ [89, 90], a second detector at the magic baseline [77, 91, 92] or a lower threshold (see [79]).

4. Sensitivity to CP violation

Due to the continuous intrinsic $\sin^2 2\theta_{13}$-$\delta_{\rm CP}$-degeneracy a total rates analysis of appearance data of neutrinos only would give continuous bands as allowed regions in the $\sin^2 2\theta_{13}$-$\delta_{\rm CP}$ plane. If combined with a second band from appearance data of anti-neutrinos only two intersections, the true and the degenerate allowed region remain. Adding the spectral information obtained with conventional energy resolution, the degenerate solution can be resolved in most cases. This is the planned procedure at superbeam experiments, neutrino factories as well as beta beam experiments to resolve the $\sin^2 2\theta_{13}$-$\delta_{\rm CP}$-degeneracy. However, at a monobeam experiment only neutrino appearance is observable and the question arises, if and under which circumstances the superb energy resolution abilities of a monobeam could in principle compete in resolving the $\sin^2 2\theta_{13}$-$\delta_{\rm CP}$-degeneracy. Since we found in the last section that the ability in resolving the degeneracies does not appear until a large number of decays per year, we will fix this value to 10^{18} decays per year in all the following considerations and only discuss the fixed scenarios Setup I, Setup II, and Setup II. In figure 5 the allowed regions in the $\sin^2 2\theta_{13}$-$\delta_{\rm CP}$-plane at the 3σ confidence level are shown for different choices of input true values. This figure is for illustrative purposes only and no correlations with the other oscillation parameters is considered, i.e. they are kept fixed to the values of eq. (2.4). The left column is for Setup I (L=600km/γ = 2500), the middle column is for the Setup II (L=250km/γ = 2000), and the right column shows the allowed regions obtained for the standard neutrino factory setup for reasons of comparison. The bands, indicated by the solid grey lines, represent the corresponding allowed regions at the 3σ confidence level if only total rates are considered. As expected, the total rates allowed regions for the monobeam scenarios are bands that do not restrict $\delta_{\rm CP}$ at all whereas for the neutrino factory already also the parameter space of $\delta_{\rm CP}$ is restricted due to the information from neutrino and anti-neutrino data. If spectral information is included to the analysis, the neutrino factory allowed regions are not influenced significantly and only the small degenerate solutions can be excluded, but for the monobeam scenarios because of the superb energy resolution wide parts of the bands can be excluded and only smaller allowed regions remain that are comparable in size to the allowed regions from the neutrino factory scenario. However, in some cases of choices of true values still degenerate solutions remain. As mentioned before, we have ignored correlations with the other oscillation parameters and also the sign(Δm^2_{31})-degeneracy here. In all of the further considerations, we will focus on the sensitivity to CP violation if also these correlations and all degeneracies are taken into account.

The sensitivity to any CP violation is shown in figure 6 for Setup I (upper left-hand side plot), Setup II (upper right-hand side plot), Setup II (lower left-hand side plot), and the neutrino factory scenario (lower right-hand side plot) at the 1, 2, 3, 4, and 5 σ confidence

JHEP08(2007)079

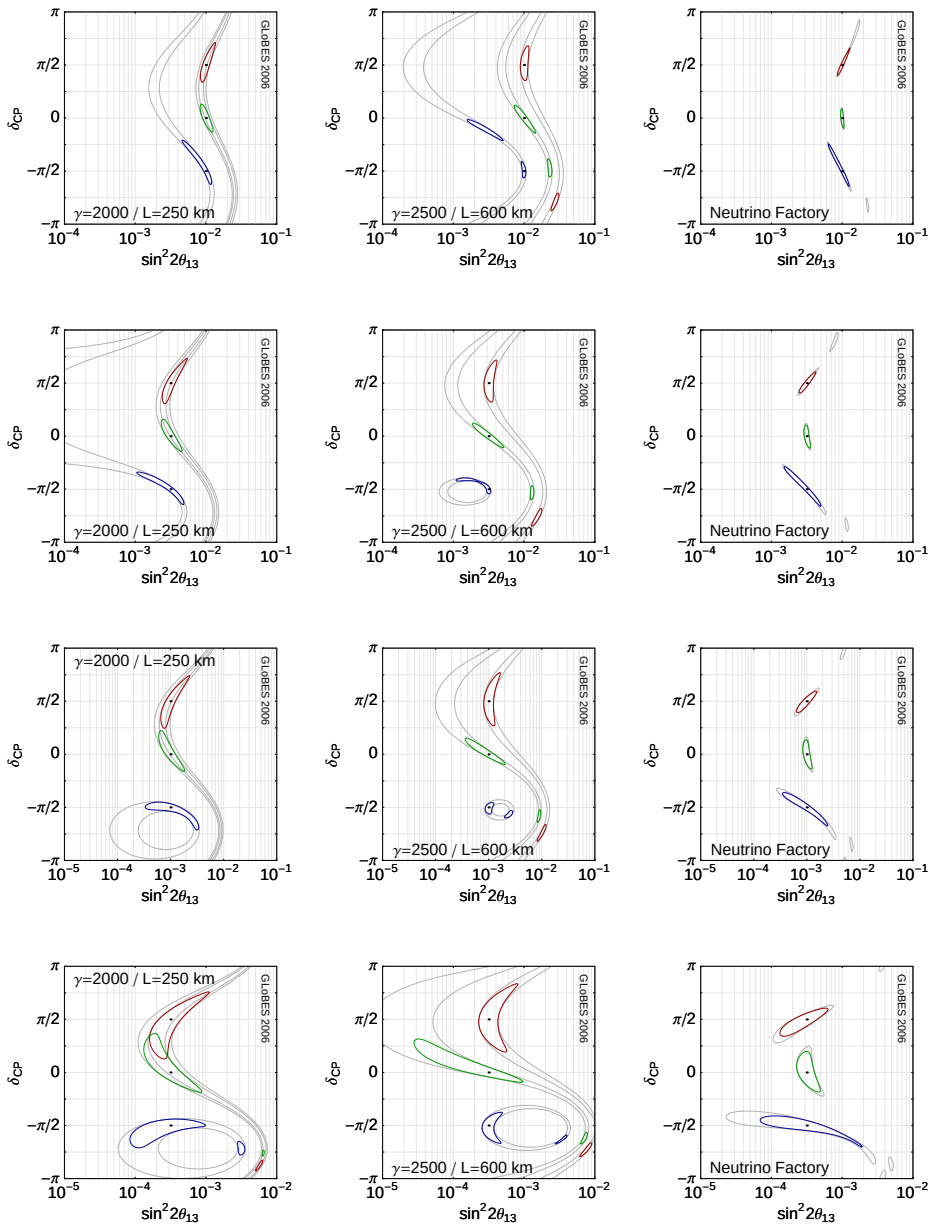

Figure 5: The allowed regions in the $\sin^2 2\theta_{13}$-$\delta_{\rm CP}$-plane for the true values indicated by the black dots at 3σ for Setup I (left column), Setup II (middle column), and a standard neutrino factory (right column) for reasons of comparison. Only the correlation between $\sin^2 2\theta_{13}$ and $\delta_{\rm CP}$ are taken into account and all other parameters are fixed to values of eq. (2.4). The plots also contain the allowed regions at 3σ for total rates only (grey solid lines).

level from bright grey/yellow (1σ) to red/dark grey (5σ). Sensitivity to any CP violation is given for a pair of true values $\sin^2 2\theta_{13}$-$\delta_{\rm CP}$ if the CP conserving values $\delta_{\rm CP} = 0$ and

JHEP08(2007)079

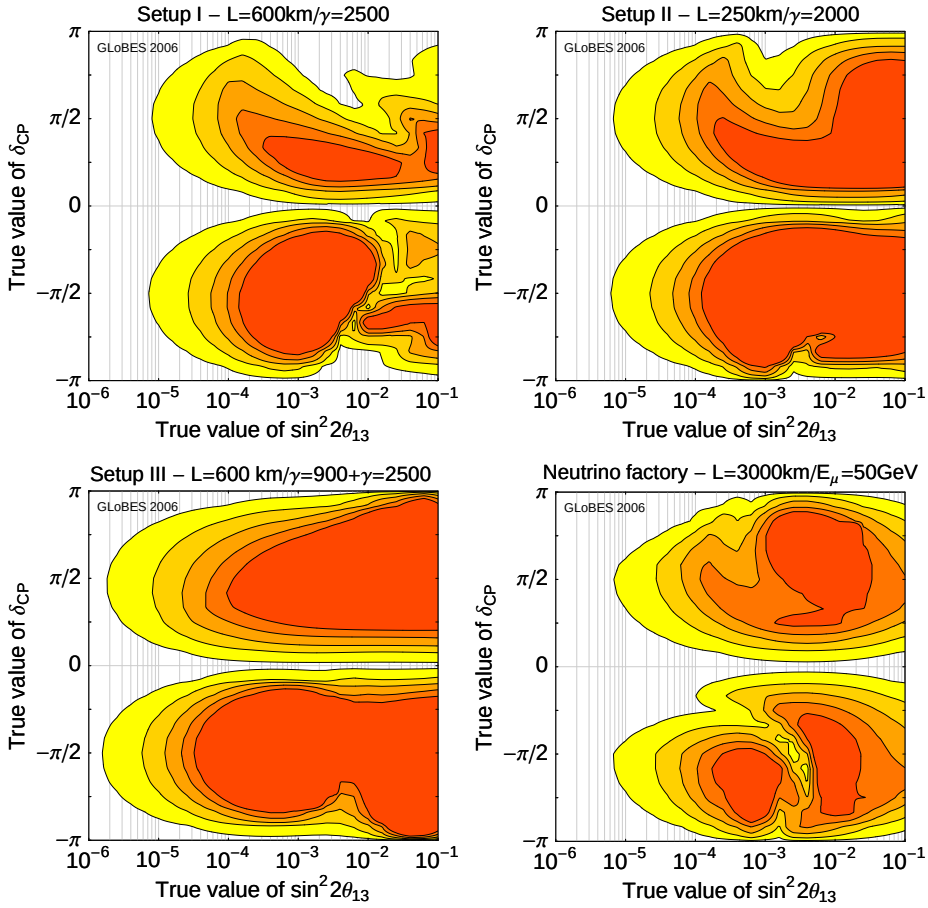

Figure 6: Sensitivity to any CP violation at 1 (yellow/bright grey), 2, 3, 4, and 5σ (red/dark grey) after 10 years of data taking as a function of the true values of $\sin^2 2\theta_{13}$ and $\delta_{\rm CP}$. The sensitivities are shown for the monobeam scenarios Setup I (upper left-hand side plot), Setup I (upper right-hand side plot), Setup III (lower left-hand side plot) and a standard neutrino factory (lower right-hand side plot) for reasons of comparison. For a pair of true values within the shaded regions the CP conserving fit values $\delta_{\rm CP} = 0$ and $\delta_{\rm CP} = \pi$ can be excluded at the respective confidence level.

$\delta_{\rm CP} = \pi$ do not fit the simulated reference data if all correlations and degeneracies are taken into account. It is known, that the standard neutrino factory suffers from the sign(Δm^2_{31})-degeneracy in some areas of the parameter space ($\sin^2 2\theta_{13} \approx 10^{-2.5}$ and $\delta_{\rm CP} \approx -\pi/2$), because of the so-called "π-transit", i.e. the degenerate solution fitted with wrong sign of Δm^2_{31} contains the CP conserving value for $\delta_{\rm CP} = \pi$ (see [49] for details). As can be seen from figure 6, Setup I suffers strongly from correlations and degeneracies at larger true values of $\sin^2 2\theta_{13}$ whereas Setup II performs better. Within the interval $\delta_{\rm CP} \in [-\pi, 0]$ Setup II does not suffer from any correlations and degeneracies anymore and gives better results than the neutrino factory in the same interval. In the interval $\delta_{\rm CP} \in [0, \pi]$ Setup II and the neutrino factory perform in a comparable manner, only for larger true values of $\sin^2 2\theta_{13} \gtrsim 10^{-2}$ the neutrino factory looses sensitivity to CP violation for values of

JHEP08(2007)079

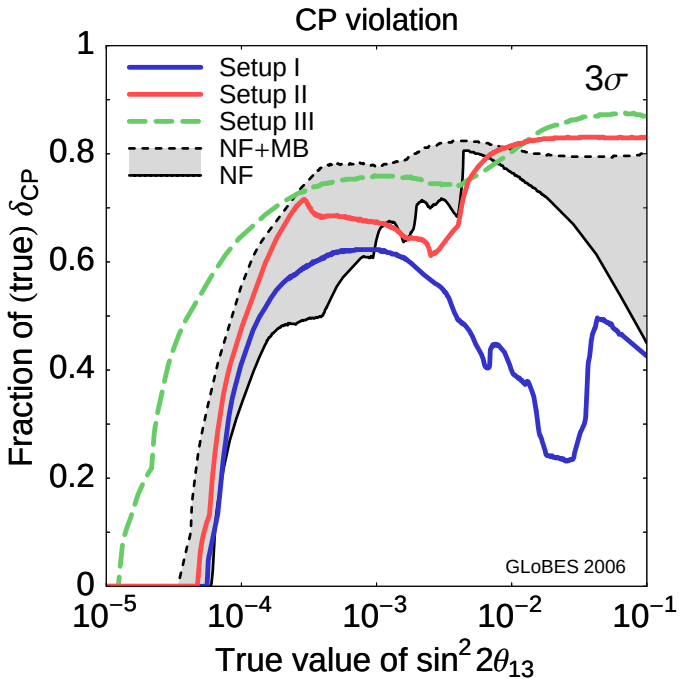

Figure 7: Comparison of the fraction of (true) $\delta_{\rm CP}$ for which CP violation can be established at the 3σ confidence level as a function of the true value of $\sin^2 2\theta_{13}$ at the monobeam scenarios Setup I, Setup II, Setup III. The solid black line is for a standard neutrino factory while the dashed line is for an optimized neutrino factory with a second detector at the magic baseline.

$\delta_{\rm CP}$ near the CP conserving values. This effect is due to the uncertainty of the matter density along the baseline which strongly affects the performance of a neutrino factory at large values of $\sin^2 2\theta_{13}$ because of the very long baseline. The best sensitivity to any CP violation is found for Setup III. Here, the combination of data from the first and second oscillation maximum can resolve the degeneracies that appear at the baseline of L=600km for Setup I. Additionally the sensitivity to CP violation of Setup III reaches to significant smaller values of $\sin^2 2\theta_{13}$ at the maximally CP violating values $\delta_{\rm CP} = \pm\pi/2$. We checked that, as also was the case for sensitivity to $\sin^2 2\theta_{13}$, a combination of 2 years at $\gamma = 900$ and 8 years at $\gamma = 2500$ would also already allow to give this performance. The results from figure 6 are finally summarized in figure 7. The fraction of $\delta_{\rm CP}$ parameter space where sensitivity to any CP violation is given at the 3σ confidence level is shown as a function of true $\sin^2 2\theta_{13}$ for the considered scenarios Setup I, Setup II, Setup III and a neutrino factory. The performance of the standard neutrino factory is indicated by the black solid line. However, we also show the performance of an optimized neutrino factory scenario, where in addition to the standard golden channel measurements at the baseline $L \sim 3000$km a second 50kt Magnetized detector is installed approximately at the magic baseline $L = 7500$km. As can be seen in figure 7, the performance of the neutrino factory setup is significantly improved. Note, that a CP fraction of 1 can never be achieved, since values near the CP conserving values can never be distinguished due to finite statistics.

JHEP08(2007)079

5. Summary and conclusions

We have analyzed the potential of high gamma neutrino beams from electron capture decays of $^{110}_{50}$Sn isotopes directed towards a large Water Cherenkov detector with a fiducial mass of 500 kt. The resulting neutrino beam would be completely flavor pure and only consist of electron neutrinos. The achievable resolution in the energy reconstruction in such a scenario can be significantly more precise than from the usual energy reconstruction in Water Cherenkov detectors, since it is performed by the position measurement within the detector. The aim of this work was to estimate the potential and requirements of such scenarios to resolve the correlations and degeneracies in the sensitivity to $\sin^2 2\theta_{13}$ and the sensitivity to any CP violation, only with their power in energy resolution abilities. This has been compared to the performance at a neutrino factory, where the combination of neutrino- and anti-neutrino running is used to resolve correlations and degeneracies. We have compared three monobeam setups, two of them with a different energy window at different locations respective to the first oscillation maximum. Setup I at a baseline of L=600km and $\gamma = 2500$ has been chosen such, that the energy window of the analysis is directly located at the first oscillation maximum, but due to this choice the energy window is not broad enough to cover the whole oscillation maximum. Setup II at a baseline of L=250km and $\gamma = 2000$ on the other hand has a broader energy window which is located at higher energies as the oscillation maximum. In comparison to Setup I this setup gains from the broader energy window and the larger statistics due to the smaller baseline. The baseline of L=600km also allows to take data at the second oscillation maximum, which is at this baseline already located at energies above the Cherenkov threshold of muons. Therefore Setup III combines a measurement at the first oscillation maximum ($\gamma = 2500$ as in Setup I) and the second oscillation maximum ($\gamma = 900$), 5 years data taking each. For the exposure of the setups it has been assumed to have a running time of 10 years at a number of 10^{18} decays per year. This number is hard to obtain because of the relative long lifetime of the $^{110}_{50}$Sn isotopes and an enhancement of the electron capture rate has to be achieved. However, concerning the sensitivity to $\sin^2 2\theta_{13}$ we found that this number is required to evolve capabilities to start resolving the correlations but still the pure superb energy resolution and the high statistics alone cannot compete with the sensitivity to $\sin^2 2\theta_{13}$ at a standard neutrino factory with a 50 kt MID detector at a baseline of L=3000km and a parent muon energy of $E_\mu = 50$GeV because the degeneracies cannot completely be resolved. On the other hand the neutrino factory also suffers strongly from degeneracies and additional data from the silver channel, the magic baseline or lower energies (maybe with a hybrid detector) would be required. Setup III on the other hand with the combination of data from first and second oscillation maximum performs well in resolving the correlations and degeneracies. It gives a better sensitivity $\sin^2 2\theta_{13} \lesssim 2.5 \cdot 10^{-4}$ at the 3σ confidence level. When it comes to the sensitivity to any CP violation the performance of the monobeam setups is more impressive than the performance concerning the sensitivity to $\sin^2 2\theta_{13}$. Setup I still suffers significantly from the degeneracies while Setup II reaches sensitivity in a quite large part of the parameter space and no negative effects from degeneracies could be observed. Finally, Setup III showed very good abilities

JHEP08(2007)079

to establish CP violation in a very large part of the parameter space and all degeneracies coming from the measurement in Setup I can be resolved due to the data from the second oscillation maximum although no information from a anti-neutrino running is included. However, one has to note that the requirements to achieve such a performance, i.e. the very large acceleration factors of the isotopes, the high number of isotope decays per year, and the very low beam divergence of the stored isotopes of $\mathcal{O}(1\ \mu\text{rad})$ are extreme.

Acknowledgments

M. R. would like to thank Marc-Thomas Eisele for useful discussions. M. R. is supported by the Graduiertenkolleg 1054 of Deutsche Forschungsgemeinschaft. J. S. is partially supported by Grant-in-Aid for Scientific Research on Priority Area No. 1774013 and No. 18034001.

A. Relativistic transformations

A.1 Neutrino energy

In the following considerations, the primed quantities are defined as the quantities in the laboratory frame, i.e. the rest frame of the detector and the quantities without a prime represent those in the rest frame of the electron capture decays in which the neutrinos are produced.

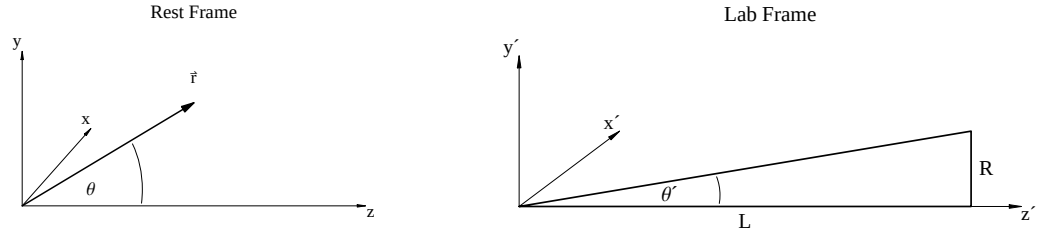

In the rest frame of the decays the neutrinos are produced at an energy Q and with an uniform angular distribution of momentum. Since for the considered mother nuclei $^{110}_{50}$Sn the endpoint energy is Q = 267 keV ($m_\nu \ll Q$), the neutrino mass can be neglected:

$$Q^2 = p^2 + m^2 \approx p^2. \tag{A.1}$$

So, for a neutrino that is emitted in the direction $\vec{r}$ the four-momentum in the rest frame of the decay is given by

$$p^\mu = \begin{pmatrix} Q \\ \\ Q\vec{e}_r \\ \\ \end{pmatrix} = \begin{pmatrix} Q \\ Q\ \sin\theta\ \cos\phi \\ Q\ \sin\theta\ \sin\phi \\ Q\ \cos\theta \end{pmatrix}. \tag{A.2}$$

Since the problem is ϕ-symmetric, we can choose $\phi = 0$ for the sake of simplicity and the four-momentum of the neutrino in the rest frame can be written as

$$p^{\mu} = \begin{pmatrix} Q \\ Q\ \sin\theta \\ 0 \\ Q\ \cos\theta \end{pmatrix}. \tag{A.3}$$

The boost is in the z-direction, and after the transformation the energy of the neutrino in the lab frame becomes

$$E' = p'^0 = \gamma\, Q(1 + \beta\, \cos\theta). \tag{A.4}$$

A.2 Transformation of angles

Now we want to derive the energy of a neutrino that hits the detector at a baseline L and at the distance R from the beam center, i.e. at an angle

$$\cos\theta' = \frac{L}{\sqrt{L^2 + R^2}} = \frac{1}{\sqrt{1 + (L/R)^2}}. \tag{A.5}$$

The expression for the neutrino energy has to be found as a function of the angle $\cos\theta'$, or respectively the radius R.

From $p^{\mu'}$ it is quite straight forward to find the transformation of $\cos\theta$:

$$\cos\theta' = \frac{\gamma Q(\beta + \cos\theta)}{\sqrt{(\gamma Q(\beta + \cos\theta))^2 + (Q\sin\theta)^2}} = \frac{\beta + \cos\theta}{1 + \beta\cos\theta} \tag{A.6}$$

and in the other direction the transformation is given by

$$\cos\theta = \frac{-\beta + \cos\theta'}{1 - \beta\cos\theta'}. \tag{A.7}$$

The transformation of ϕ is trivial $\phi = \phi'$ and therefore we find that

$$\frac{d\Omega}{d\Omega'} = \frac{d\cos\theta}{d\cos\theta'} \tag{A.8}$$

with

$$\frac{d\cos\theta}{d\cos\theta'} = \left[\gamma^2(1 - \beta\cos\theta')^2\right]^{-1} \tag{A.9}$$

and the corresponding

$$\frac{d\cos\theta'}{d\cos\theta} = \left[\gamma^2(1 + \beta\cos\theta)^2\right]^{-1}. \tag{A.10}$$

Now, the exact formula for the neutrino energy in the lab frame as a function of the lab frame quantities is found to be:

$$E'(\cos\theta') = \frac{Q}{\gamma}\frac{1}{1 - \beta\cos\theta'} \tag{A.11}$$

and

$$E'(R) = \frac{Q}{\gamma}\left[1 - \frac{\beta}{\sqrt{1 + (R/L)^2}}\right]^{-1}. \tag{A.12}$$

B. Calculation of event rates

The initial neutrino beam consists only of electron neutrinos. In the detector the muon neutrinos from the appearance channel will be detected. The neutrino energy is maximal at the beam center ($R = 0$) with $E_{\max} = 2\gamma Q$ and decreases to the outer regions of the detector. We introduce an equidistant binning in R^2 to have more balanced event numbers in the different bins, than would be the case for equidistant binning in R. In the simulations, we use $k = 100$ bins, so that the largest bin appears in the beam center with approximately 10 m radius and the smallest bin is found at the outer edge of the detector with a width of approximately 50 cm, whereas the position measurement resolution is assumed to be at least 30 cm, which is the vertex resolution estimated for fully-contained single ring events at Super-K [14] in the energy window of interest. In this work we have not introduced an additional smearing between the bins in the outer regions of the detector. However, if the vertex resolution cannot be optimized this binning turns out to be too narrow at the outer bins in the detector and smearing would have to be introduced to these bins or the width of the bins in the analysis would have to be customized. We checked, that going to an equidistant binning in R^2 with only 50 bins, i.e. bin sizes from 14 m to 1 m, or going to an equidistant binning in R with 100 bins hardly changes the main results of this work.

For the usage within the GLoBES software, the radial binning is translated to binning in energy, where the bins are not equidistant anymore.

If $R^2_{\max}$ is divided in k bins the edges of the bins are

$$R_i^2 = R^2_{\max} - (i-1)\Delta R^2 \tag{B.1}$$

with

$$\Delta R^2 = \frac{R^2_{\max}}{k}. \tag{B.2}$$

Here always $R_i^2 > R_{i+1}^2$ holds, so that the corresponding energy bins are in the right ordering for GLoBES :

$$E'(R_i^2) < E'(R_{i+1}^2). \tag{B.3}$$

Furthermore, within GLoBES for the calculations the mean value of each energy bin is taken:

$$E_i = \frac{E'(R_i^2) + E'(R_{i+1}^2)}{2}. \tag{B.4}$$

Then, the appearance event number in one energy-bin is given by

$$N_i \simeq \epsilon_i \times P(L, E_i)_{\nu_e \to \nu_\mu} \times \frac{1}{L^2} \frac{dn}{d\Omega'}(E_i') \times \sigma(E_i') \times N_{\text{nuc,i}}, \tag{B.5}$$

where ϵ_i is the signal efficiency in the corresponding bin, $P(L, E_i)_{\nu_e \to \nu_\mu}$ is the appearance oscillation probability, $\frac{dn}{d\Omega'}(E_i')$ is the angular neutrino flux, $\sigma(E_i')$ is the charged current

cross section per nucleon, and $N_{\mathrm{nuc,i}}$ is the number of nucleons within the geometrical size of the i-th bin:

$$N_{\mathrm{nuc,i}} = \Gamma_i \times \frac{M_{\mathrm{det}}}{m_{\mathrm{nuc}}} = \frac{1}{R_{\mathrm{max}}^2}\left[R_i^2 - R_{i+1}^2\right] \times \frac{M_{\mathrm{det}}}{m_{\mathrm{nuc}}} = \frac{1}{k} \times \frac{M_{\mathrm{det}}}{m_{\mathrm{nuc}}}. \tag{B.6}$$

Here Γ_i is the fraction of all number of nucleons that have to be considered in the i-th energy bin.

Since the neutrino flux in the rest frame of the decays is uniformly distributed, it can be written as

$$\frac{dn}{d\Omega} = \frac{N_{\mathrm{decays}}}{4\pi}, \tag{B.7}$$

where N_{decays} is just the number of decays, i.e. the number of produced neutrinos. The neutrino flux can now be found with eqs. (A.9) and (A.11):

$$\frac{dn}{d\Omega'_i} = \frac{dn}{d\Omega}\frac{d\Omega}{d\Omega'} = \frac{N_{\mathrm{decays}}}{4\pi}\left[\gamma^2(1-\beta\cos\theta'_i)^2\right]^{-1} = \frac{N_{\mathrm{decays}}}{4\pi}\left(\frac{E'_i}{Q}\right)^2. \tag{B.8}$$

Also, it is straight forward to show by using eqs. (A.8), (A.9), (A.11), and (B.7) that

$$dn = \frac{dn}{d\Omega}\frac{d\Omega}{d\Omega'}\frac{d\Omega'}{dE'}dE' = \frac{N_{\mathrm{decays}}}{2\beta\gamma Q}dE', \tag{B.9}$$

i.e. $\frac{dn}{dE'}$ is constant.

References

[1] B.T. Cleveland et al., *Measurement of the solar electron neutrino flux with the homestake chlorine detector*, *Astrophys. J.* **496** (1998) 505.

[2] SAGE collaboration, J.N. Abdurashitov et al., *Measurement of the solar neutrino capture rate by the russian-american gallium solar neutrino experiment during one half of the* 22*-year cycle of solar activity*, *J. Exp. Theor. Phys.* **95** (2002) 181 [astro-ph/0204245].

[3] GALLEX collaboration, W. Hampel et al., *Gallex solar neutrino observations: results for Gallex IV*, *Phys. Lett.* **B 447** (1999) 127.

[4] GNO collaboration, M. Altmann et al., *GNO solar neutrino observations: results for GNO I*, *Phys. Lett.* **B 490** (2000) 16 [hep-ex/0006034].

[5] Super-Kamiokande collaboration, S. Fukuda et al., *Constraints on neutrino oscillations using* 1258 *days of Super-Kamiokande solar neutrino data*, *Phys. Rev. Lett.* **86** (2001) 5656 [hep-ex/0103033].

[6] Super-Kamiokande collaboration, S. Fukuda et al., *Solar B*8 *and He p neutrino measurements from* 1258 *days of Super-Kamiokande data*, *Phys. Rev. Lett.* **86** (2001) 5651 [hep-ex/0103032].

[7] Super-Kamiokande collaboration, S. Fukuda et al., *Determination of solar neutrino oscillation parameters using* 1496 *days of Super-Kamiokande-I data*, *Phys. Lett.* **B 539** (2002) 179 [hep-ex/0205075].

JHEP08(2007)079

[8] SNO collaboration, Q.R. Ahmad et al., *Measurement of day and night neutrino energy spectra at SNO and constraints on neutrino mixing parameters*, *Phys. Rev. Lett.* **89** (2002) 011302 [nucl-ex/0204009].

[9] SNO collaboration, Q.R. Ahmad et al., *Direct evidence for neutrino flavor transformation from neutral-current interactions in the sudbury neutrino observatory*, *Phys. Rev. Lett.* **89** (2002) 011301 [nucl-ex/0204008].

[10] SNO collaboration, S.N. Ahmed et al., *Measurement of the total active B-8 solar neutrino flux at the sudbury neutrino observatory with enhanced neutral current sensitivity*, *Phys. Rev. Lett.* **92** (2004) 181301 [nucl-ex/0309004].

[11] Super-Kamiokande collaboration, Y. Fukuda et al., *Evidence for oscillation of atmospheric neutrinos*, *Phys. Rev. Lett.* **81** (1998) 1562 [hep-ex/9807003].

[12] Super-Kamiokande collaboration, Y. Fukuda et al., *Measurement of the flux and Zenith-angle distribution of upward through-going muons by Super-Kamiokande*, *Phys. Rev. Lett.* **82** (1999) 2644 [hep-ex/9812014].

[13] Super-Kamiokande collaboration, S. Fukuda et al., *Tau neutrinos favored over sterile neutrinos in atmospheric muon neutrino oscillations*, *Phys. Rev. Lett.* **85** (2000) 3999 [hep-ex/0009001].

[14] Super-Kamiokande collaboration, Y. Ashie et al., *A measurement of atmospheric neutrino oscillation parameters by super-kamiokande i*, *Phys. Rev.* **D 71** (2005) 112005 [hep-ex/0501064].

[15] MACRO collaboration, M. Ambrosio et al., *Measurement of the atmospheric neutrino-induced upgoing muon flux using macro*, *Phys. Lett.* **B 434** (1998) 451 [hep-ex/9807005].

[16] F. Ronga, *Atmospheric neutrinos in the Soudan-2 and macro experiments*, *Nucl. Phys.* **100** *(Proc. Suppl.)* (2001) 113.

[17] Soudan 2 collaboration, M.C. Sanchez et al., *Observation of atmospheric neutrino oscillations in Soudan 2*, *Phys. Rev.* **D 68** (2003) 113004 [hep-ex/0307069].

[18] MACRO collaboration, M. Ambrosio et al., *Measurements of atmospheric muon neutrino oscillations, global analysis of the data collected with macro detector*, *Eur. Phys. J.* **C 36** (2004) 323.

[19] KamLAND collaboration, K. Eguchi et al., *First results from KamLAND: evidence for reactor anti-neutrino disappearance*, *Phys. Rev. Lett.* **90** (2003) 021802 [hep-ex/0212021].

[20] KamLAND collaboration, T. Araki et al., *Measurement of neutrino oscillation with KamLAND: evidence of spectral distortion*, *Phys. Rev. Lett.* **94** (2005) 081801 [hep-ex/0406035].

[21] Z. Maki, M. Nakagawa and S. Sakata, *Remarks on the unified model of elementary particles*, *Prog. Theor. Phys.* **28** (1962) 870.

[22] K2K collaboration, M.H. Ahn et al., *Indications of neutrino oscillation in a 250 Km long-baseline experiment*, *Phys. Rev. Lett.* **90** (2003) 041801 [hep-ex/0212007].

[23] Y. Oyama, *Results from K2K and status of T2K*, hep-ex/0512041.

[24] K2K collaboration, M.H. Ahn et al., *Measurement of neutrino oscillation by the K2K experiment*, *Phys. Rev.* **D 74** (2006) 072003 [hep-ex/0606032].

JHEP08(2007)079

[25] MINOS collaboration, N. Tagg, *First minos results from the NuMi beam*, hep-ex/0605058.

[26] MINOS collaboration, D.G. Michael et al., *Observation of muon neutrino disappearance with the minos detectors and the NuMi neutrino beam*, *Phys. Rev. Lett.* **97** (2006) 191801 [hep-ex/0607088].

[27] CHOOZ collaboration, M. Apollonio et al., *Limits on neutrino oscillations from the CHOOZ experiment*, *Phys. Lett.* **B 466** (1999) 415 [hep-ex/9907037].

[28] CHOOZ collaboration, M. Apollonio et al., *Search for neutrino oscillations on a long base-line at the CHOOZ nuclear power station*, *Eur. Phys. J.* **C 27** (2003) 331 [hep-ex/0301017].

[29] H. Minakata, H. Sugiyama, O. Yasuda, K. Inoue and F. Suekane, *Reactor measurement of θ_{13} and its complementarity to long-baseline experiments*, *Phys. Rev.* **D 68** (2003) 033017 [hep-ph/0211111].

[30] P. Huber, M. Lindner, T. Schwetz and W. Winter, *Reactor neutrino experiments compared to superbeams*, *Nucl. Phys.* **B 665** (2003) 487 [hep-ph/0303232].

[31] K. Anderson et al., *White paper report on using nuclear reactors to search for a value of θ_{13}*, hep-ex/0402041.

[32] F. Ardellier et al., *Letter of intent for Double-CHOOZ: a search for the mixing angle θ_{13}*, hep-ex/0405032.

[33] Double Chooz collaboration, F. Ardellier et al., *Double CHOOZ: a search for the neutrino mixing angle θ_{13}*, hep-ex/0606025.

[34] P. Huber, J. Kopp, M. Lindner, M. Rolinec and W. Winter, *From Double CHOOZ to Triple CHOOZ: neutrino physics at the CHOOZ reactor complex*, *JHEP* **05** (2006) 072 [hep-ph/0601266].

[35] H. Minakata and H. Nunokawa, *Measuring leptonic CP-violation by low energy neutrino oscillation experiments*, *Phys. Lett.* **B 495** (2000) 369 [hep-ph/0004114].

[36] J. Sato, *Neutrino oscillation and CP-violation*, *Nucl. Instrum. Meth.* **A472** (2001) 434 [hep-ph/0008056].

[37] B. Richter, *Conventional beams or neutrino factories: the next generation of accelerator-based neutrino experiments*, hep-ph/0008222.

[38] MINOS collaboration, E. Ables et al., FERMILAB-PROPOSAL-P-875.

[39] The T2K collaboration, Y. Itow et al., *The JHF-Kamioka neutrino project*, hep-ex/0106019.

[40] NOvA collaboration, I. Ambats et al., FERMILAB-PROPOSAL-0929.

[41] S. Geer, *Neutrino beams from muon storage rings: characteristics and physics potential*, *Phys. Rev.* **D 57** (1998) 6989 [hep-ph/9712290].

[42] A. De Rujula, M.B. Gavela and P. Hernandez, *Neutrino oscillation physics with a neutrino factory*, *Nucl. Phys.* **B 547** (1999) 21 [hep-ph/9811390].

[43] K. Dick, M. Freund, M. Lindner and A. Romanino, *CP-violation in neutrino oscillations*, *Nucl. Phys.* **B 562** (1999) 29 [hep-ph/9903308].

JHEP08(2007)079

[44] V.D. Barger, S. Geer and K. Whisnant, *Long baseline neutrino physics with a muon storage ring neutrino source*, *Phys. Rev.* **D 61** (2000) 053004 [hep-ph/9906487].

[45] A. Cervera et al., *Golden measurements at a neutrino factory*, *Nucl. Phys.* **B 579** (2000) 17 [hep-ph/0002108].

[46] C.H. Albright et al., *Physics at a neutrino factory*, hep-ex/0008064.

[47] A. Blondel et al., *Contribution to the NuFact'99 workshop, 5-9 July (1999) Lyon — France*, *Nucl. Instrum. Meth. A* **451** (2000) 102.

[48] M. Apollonio et al., *Oscillation physics with a neutrino factory*, hep-ph/0210192.

[49] P. Huber, M. Lindner and W. Winter, *Superbeams versus neutrino factories*, *Nucl. Phys.* **B 645** (2002) 3 [hep-ph/0204352].

[50] P. Zucchelli, *A novel concept for a anti-$\nu/e/\nu/e$ neutrino factory: the β beam*, *Phys. Lett.* **B 532** (2002) 166.

[51] M. Mezzetto, *Physics reach of the β beam*, *J. Phys.* **G 29** (2003) 1771 [hep-ex/0302007].

[52] J. Bouchez, M. Lindroos and M. Mezzetto, *β beams: present design and expected performances*, *AIP Conf. Proc.* **721** (2004) 37 [hep-ex/0310059].

[53] M. Mezzetto, *β beams*, *Nucl. Phys.* **143** *(Proc. Suppl.)* (2005) 309 [hep-ex/0410083].

[54] J. Burguet-Castell, D. Casper, J.J. Gomez-Cadenas, P. Hernandez and F. Sanchez, *Neutrino oscillation physics with a higher $\gamma\beta$-beam*, *Nucl. Phys.* **B 695** (2004) 217 [hep-ph/0312068].

[55] J. Burguet-Castell, D. Casper, E. Couce, J.J. Gomez-Cadenas and P. Hernandez, *Optimal β-beam at the CERN-SPS*, *Nucl. Phys.* **B 725** (2005) 306 [hep-ph/0503021].

[56] F. Terranova, A. Marotta, P. Migliozzi and M. Spinetti, *High energy β beams without massive detectors*, *Eur. Phys. J.* **C 38** (2004) 69 [hep-ph/0405081].

[57] A. Donini, E. Fernandez-Martinez, P. Migliozzi, S. Rigolin and L. Scotto Lavina, *Study of the eightfold degeneracy with a standard β-beam and a super-beam facility*, *Nucl. Phys.* **B 710** (2005) 402 [hep-ph/0406132].

[58] A. Donini, E. Fernandez-Martinez and S. Rigolin, *Appearance and disappearance signals at a β-beam and a super-beam facility*, *Phys. Lett.* **B 621** (2005) 276 [hep-ph/0411402].

[59] A. Donini and E. Fernandez-Martinez, *Alternating ions in a β-beam to solve degeneracies*, *Phys. Lett.* **B 641** (2006) 432 [hep-ph/0603261].

[60] A. Donini et al., *A β beam complex based on the machine upgrades of the LHC*, *Eur. Phys. J.* **C 48** (2006) 787 [hep-ph/0604229].

[61] P. Huber, M. Lindner, M. Rolinec and W. Winter, *Physics and optimization of β-beams: from low to very high γ*, *Phys. Rev.* **D 73** (2006) 053002 [hep-ph/0506237].

[62] J.E. Campagne, M. Maltoni, M. Mezzetto and T. Schwetz, *Physics potential of the cern-memphys neutrino oscillation project*, *JHEP* **04** (2007) 003 [hep-ph/0603172].

[63] C. Volpe, *Topical review on 'β-beams'*, *J. Phys.* **G 34** (2007) 1 [hep-ph/0605033].

[64] J. Sato, *Monoenergetic neutrino beam for long baseline experiments*, *Phys. Rev. Lett.* **95** (2005) 131804 [hep-ph/0503144].

JHEP08(2007)079

[65] J. Bernabeu, J. Burguet-Castell, C. Espinoza and M. Lindroos, *Monochromatic neutrino beams*, *JHEP* **12** (2005) 014 [hep-ph/0505054].

[66] J. Sato, *Monoenergetic neutrino beam for long baseline experiments*, *Nucl. Phys.* **155** *(Proc. Suppl.)* (2006) 180.

[67] M. Lindroos, J. Bernabeu, J. Burguet-Castell and C. Espinoza, *Measurements of azimutal asymmetries in netural current deep inelastic scattering aqt HERA*, PoS(HEP2005)365.

[68] J. Bernabeu, J. Burguet-Castell, C. Espinoza and M. Lindroos, *Perspectives in neutrino physics: monochromatic neutrino beams*, hep-ph/0512299.

[69] J. Bernabeu, J. Burguet-Castell and C. Espinoza, *Physics reach with a monochromatic neutrino beam from electron capture*, PoS(HEP2005)182 [hep-ph/0512297].

[70] J. Bernabeu, J. Burguet-Castell, C. Espinoza and M. Lindroos, *Physics reach of electron-capture neutrino beams*, *Nucl. Phys.* **155** *(Proc. Suppl.)* (2006) 222 [hep-ph/0510278].

[71] M. Ikeda, I. Nakano, M. Sakuda, R. Tanaka and M. Yoshimura, *New method of enhancing lepton number nonconservation*, hep-ph/0506062.

[72] M. Yoshimura, *Photon irradiated compression as a tool of investigating fundamental physics beyond standard model*, hep-ph/0507248.

[73] T. Nomura, J. Sato and T. Shimomura, *Laser irradiated enhancement of atomic electron capture rate in search of new physics*, *Prog. Theor. Phys.* **117** (2007) 401 [hep-ph/0605031].

[74] TOTEM collaboration, M. Deile, *Totem: forward physics at the LHC*, hep-ex/0410084.

[75] M. Koike, T. Ota and J. Sato, *Ambicuities of theoretical parameters and CP or T violation in neutrino factories*, *Phys. Rev.* **D 65** (2002) 053015 [hep-ph/0011387].

[76] H. Minakata and H. Nunokawa, *Exploring neutrino mixing with low energy superbeams*, *JHEP* **10** (2001) 001 [hep-ph/0108085].

[77] V. Barger, D. Marfatia and K. Whisnant, *Breaking eight-fold degeneracies in neutrino CP-violation, mixing and mass hierarchy*, *Phys. Rev.* **D 65** (2002) 073023 [hep-ph/0112119].

[78] J. Arafune, M. Koike and J. Sato, *CP-violation and matter effect in long baseline neutrino oscillation experiments*, *Phys. Rev.* **D 56** (1997) 3093 [hep-ph/9703351].

[79] P. Huber, M. Lindner, M. Rolinec and W. Winter, *Optimization of a neutrino factory oscillation experiment*, *Phys. Rev.* **D 74** (2006) 073003 [hep-ph/0606119].

[80] P. Huber, M. Lindner and W. Winter, *Simulation of long-baseline neutrino oscillation experiments with globes*, *Comput. Phys. Commun.* **167** (2005) 195 [hep-ph/0407333].

[81] M. Rolinec, *GLoBES and its application to neutrino physics*, *Acta Phys. Polon. B* **37** (2006) 2049.

[82] *GLoBES manual* online at arXiv:http://www.ph.tum.de/~globes (2004).

[83] G.L. Fogli, E. Lisi, A. Marrone and D. Montanino, *Status of atmospheric $\nu_\mu \to$ nu/tau oscillations and decoherence after the first k2k spectral data*, *Phys. Rev.* **D 67** (2003) 093006 [hep-ph/0303064].

[84] M. Maltoni, T. Schwetz, M.A. Tortola and J.W.F. Valle, *Status of global fits to neutrino oscillations*, *New J. Phys.* **6** (2004) 122 [hep-ph/0405172].

JHEP08(2007)079

[85] J.N. Bahcall, M.C. Gonzalez-Garcia and C. Pena-Garay, *Solar neutrinos before and after neutrino 2004*, *JHEP* **08** (2004) 016 [hep-ph/0406294].

[86] A. Bandyopadhyay, S. Choubey, S. Goswami, S.T. Petcov and D.P. Roy, *Update of the solar neutrino oscillation analysis with the* 766-*Ty KamLAND spectrum*, *Phys. Lett.* **B 608** (2005) 115 [hep-ph/0406328].

[87] G.L. Fogli and E. Lisi, *Tests of three-flavor mixing in long-baseline neutrino oscillation experiments*, *Phys. Rev.* **D 54** (1996) 3667 [hep-ph/9604415].

[88] J. Burguet-Castell, M.B. Gavela, J.J. Gomez-Cadenas, P. Hernandez and O. Mena, *On the measurement of leptonic CP-violation*, *Nucl. Phys.* **B 608** (2001) 301 [hep-ph/0103258].

[89] A. Donini, D. Meloni and P. Migliozzi, *The silver channel at the neutrino factory*, *Nucl. Phys.* **B 646** (2002) 321 [hep-ph/0206034].

[90] D. Autiero et al., *The synergy of the golden and silver channels at the neutrino factory*, *Eur. Phys. J.* **C 33** (2004) 243 [hep-ph/0305185].

[91] P. Lipari, *Matter effects in long-baseline experiments, the flavor content of the heaviest (or lightest) neutrino and the sign of* $\Delta(M^2)$, *Phys. Rev.* **D 61** (2000) 113004 [hep-ph/9903481].

[92] P. Huber and W. Winter, *Neutrino factories and the 'magic' baseline*, *Phys. Rev.* **D 68** (2003) 037301 [hep-ph/0301257].

JHEP08(2007)079